

Response to an applied electric field in an antiferroelectric 1/2 subphase: The role of thermal fluctuations

Koichiro Shirota^{1,*}, Atsuo Fukuda^{2,†}, Neelam Yadav,² Vitaly P. Panov^{3,2},
Jagdish K. Vij², Yutaka Yamagata,¹ and Ken Ishikawa^{4,‡}

¹RIKEN Center for Advanced Photonics (RAP), 2-1, Hirosawa, Wako, Saitama 351-0198, Japan

²Department of Electronic and Electrical Engineering, Trinity College Dublin, The University of Dublin, Dublin 2, Ireland

³Department of Electronic and Computer Engineering, Sungkyunkwan University, Suwon, Gyeonggi-do 16419, Republic of Korea

⁴Department of Materials Science and Engineering, School of Materials and Chemical Technology,
Tokyo Institute of Technology, 2-12-1 S8-28, Ookayama, Meguro-ku, Tokyo 152-8552, Japan



(Received 3 September 2022; revised 30 March 2023; accepted 27 April 2023; published 1 June 2023)

The response to an applied electric field in the $q_T = 1/2$ subphase of the MC881-MC452 binary mixture system is studied by using thick homeotropically aligned cells. In the ordinary antiferroelectric SmC_A^* and 1/2 (sub)phases, some nonplanar asymmetric distortions in the antiferroelectric unit cell structure produce induced polarization in the applied field direction, starts to unwind the helix from the beginning, and tends to align the averaged tilt plane direction parallel to the applied field. In the 1/2 subphase under consideration, however, the helix resists being deformed at the beginning and then the thresholdlike steep increase of birefringence Δn occurs in the transition from 1/2 to unwound SmC^* at a field of less than 0.5 V/ μm ; we conclude that the thermal fluctuations play an important role in promoting the director flip-flopping in a single layer under the applied field and bring about additional induced polarization, which counteracts the aforementioned ordinary induced one and prevents the helix from unwinding. This suggests that the Langevin-like director reorientation is the mechanism of the V-shaped switching which was actually observed in the thin films of Mitsui mixture [Phys. Rev. Lett. **87**, 015701 (2001)] and must have been used in prototyped thresholdless antiferroelectric liquid-crystal displays.

DOI: [10.1103/PhysRevE.107.064701](https://doi.org/10.1103/PhysRevE.107.064701)

I. INTRODUCTION

More than 20 years ago, the Inui mixture and the Mitsui mixture were reported to show the thresholdless, hysteresis-free, V-shaped switching and received enormous attention at the time for application to gray-scale liquid-crystal displays (LCDs). It was anticipated that a thresholdless antiferroelectric (TLAF) SmC^* -like phase must exist in the bulk [1–3]. Meanwhile, Rudquist *et al.* and Park *et al.* showed that the Inui mixture is ferroelectric, where the V-shaped switching is caused by the highly collective azimuthal angle rotation of the director on the tilt cone in SmC^* [4–7]. However, Seomun *et al.* [8] obtained the temperature-mixing ratio (T - r) phase diagram of constituent compounds of Mitsui mixture, **1** and **2** in Fig. 1, using thick free-standing films and thin homogeneous cells; they confirmed that the V-shaped switching in thin cells occurs even in the region where the antiferroelectric phase exists in the bulk, and that this is not due to the electric-field-induced ferroelectric state [9,10]. Moreover, Hayashi *et al.* [11,12] firmly established in thin homogeneous cells of the Mitsui mixture, by observing the Raman scattered light, that the V-shaped switching can be explained by the Langevin-like director and polarization

reorientation in antiferroelectric SmC^* -like state but not by the highly collective azimuthal angle rotation of the director on the tilt cone in ferroelectric SmC^* . Not only Mitsui Chemicals but also another Japanese chemical company, Mitsubishi Gas Chemical (MGC) [13,14], produced apparently TLAF materials. At least five groups including two Japanese companies, Casio and Toshiba, prototyped active-matrix-driven TLAF-LCDs using these materials [15–20]; they acknowledged either Mitsui Chemicals or MGC but did not show the chemical structures of the apparently TLAF materials. Moreover, we could not obtain plenty of the most likely candidate TLAF materials, enough to study their fundamental properties, from the chemical companies during active periods of developing their materials, and hence it was hard to clarify the essentials of TLAF phenomena.

Ironically, a breakthrough has come through their failure in the commercialization of TLAF materials and active-matrix-driven TLAF-LCDs. When MGC stopped the R&D of TLAF materials in 2006, they kindly donated large amounts of key compounds to one of the authors (A.F.), the chemical structural formulas of which are also shown in Fig. 1. Their basic idea is to prepare binary mixtures of antiferroelectric (**3**:MC881) and ferroelectric (**4**:MC815 or **5**:MC452) compounds and to obtain the TLAF state near the boundary [21]. Apparently, Mitsui Chemicals also adopted the same strategy; it was realized that the binary mixture boundary becomes rather parallel to the temperature axis when both antiferroelectricity and ferroelectricity are strong enough [22]. The chiral

*shirota@riken.jp

†fukudaa@tcd.ie

‡ishikawa.k.ab@m.titech.ac.jp

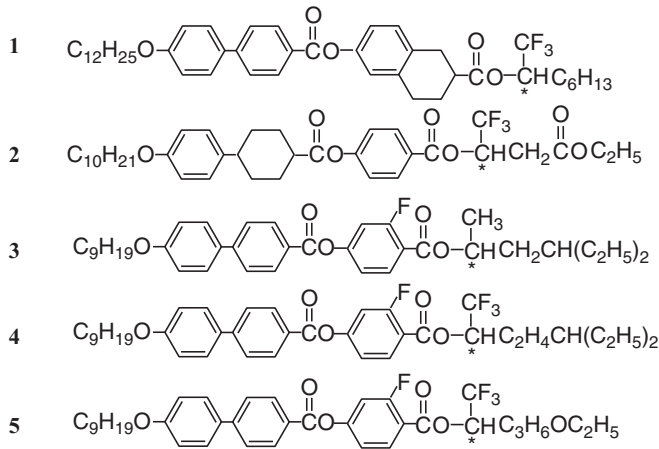


FIG. 1. Chemical structural formulas of TLAF materials. Mitsui Chemicals, Inc. reported compounds **1** and **2** as Mitsui mixture. Compounds **3**, **4**, and **5** were developed by Mitsubishi Gas Chemical (MGC), the product numbers of which are MC881, MC815, and MC452, respectively. Antiferroelectric MC881 and ferroelectric MC452 used in this paper are the (*R*) moieties. See text for details.

smectic phases of calamitic liquid crystals, SmC_A^* and SmC^* , are characterized by the synclinc ferroelectric F ordering and the anticlinic antiferroelectric A ordering in adjacent layers. The long-range interlayer interactions (LRILIs) usually lift the degeneracy of various states with mixed A and F orderings at the frustrated phase-transition point and form several subphases, for which different nomenclatures were used in the early stage of investigations when the subphase emergence mechanism was not yet clarified. Now the clinicity frustration has reasonably been understood, so the two ways of designating the subphases appear to be reasonable: one is to specify the unit cell size and the other is to use the q_T numbers given by

$$q_T = [F]/([A] + [F]), \quad (1)$$

where $[F]$ and $[A]$ are the numbers of ferroelectric and antiferroelectric orderings in the unit cell. Among them the ferrielectric subphase with the three-layer (FAA) unit cell, SmC_{d3} or $q_T = 1/3$, and the antiferroelectric subphase with the four-layer ($FAFA$) unit cell, SmC_{d4} or $q_T = 1/2$, are frequently observed. Figure 2 is the schematic illustration of these subphases. It is generally considered that the temperature-induced successive transitions via the main phases and subphases are of first order and are characterized by abrupt changes [22–28].

Sandhya *et al.* [29] noticed, however, that the change from SmC_A^* to SmC^* induced by temperature is continuous in the bulk of some binary mixtures of compounds MC881 and MC452. The phase emerging sequence is SmC_A^* - SmA -Iso in MC881, whereas it is SmC^* -Iso in MC452. As the MC452 concentration increases in the binary mixtures, apparently SmC^* comes to emerge above SmC_A^* , but the borderline between them appears to become parallel to the temperature axis at the critical concentration $r_c = 57.65 \pm 0.15$ wt.%. Sandhya *et al.* carefully studied the mixtures in the concentration range around r_c by using Bragg reflection spectra caused by the

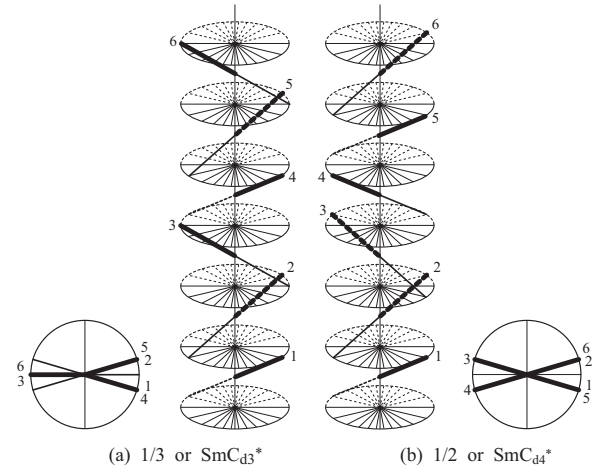


FIG. 2. Schematically illustrated directors and c-directors in the two typical biaxial subphases, where the director head and tail are represented by thick and thin lines, respectively. The subphases are characterized by nanometer-sized highly-distorted commensurate helical structures; the distortion is so large that we can still keep using Eq. (1) to designate the subphases in the following. Notice that micrometer-sized helical structures are not taken into consideration in this illustration.

director helical structure. They confirmed the emergence of an apparently single subphase with exceptionally wide temperature stability in a narrow concentration range of less than 3 wt.% adjacent to the low concentration side of r_c . The half-pitch band of SmC_A^* in pure MC881 is observed at about $0.4 \mu\text{m}$ close to the intrinsic absorption edge of the liquid crystal and that of the subphase of the mixtures appears at about $1 \mu\text{m}$. On the low concentration side of the subphase, the Bragg reflection peak wavelength characteristically becomes longer with temperature from that of apparently SmC_A^* almost buried in the intrinsic absorption edge, diverges with a change of its handedness, and decreases to attain the visible wavelength of apparently SmC^* half-pitch reflection band. On the high concentration side, however, apparently SmC^* alone emerges. In any case, the full-pitch band emerges accordingly in the apparently SmC^* temperature range, but peculiarly its emergence does not cause any discontinuous change in the half-pitch band. Even more peculiarly, it does not appear abruptly but emerges gradually; the growing temperature range becomes wider near the critical concentration r_c .

In an effort to understand the unexpected findings mentioned above, Sandhya *et al.* recognized the degeneracy lifting due to thermal fluctuations [30,31]. This is a challenge to the absolute zero temperature approximation which we usually resort to in liquid crystals: thermal transition between SmC_A^* and SmC^* can hardly occur, when these are separated by a finite potential barrier [32]. Actually, Sandhya *et al.* [29] assumed a thermal equilibrium between the synclinc and anticlinic orderings and the resulting Boltzmann distribution for the ratio between the orderings

$$[A]/[F] = \exp\{-\Delta\mathcal{E}/(k_B T)\}, \quad (2)$$

where $\Delta\mathcal{E} = \mathcal{E}_A - \mathcal{E}_F$ is usually considered to change linearly with temperature near the frustration point; it should be

noted that the thermal equilibrium is attained in a nonuniform defect-assisted way through solitary waves moving around dynamically [33]. Their analysis rather well reproduced the peculiar gradual growing of the full pitch-band as well as the characteristic temperature variation of the half-pitch band with its peak divergence in the high-temperature range around the critical concentration r_c ; it also showed that only 1% thermally excited anticlinic defects suppress the emergence of the full-pitch band in apparently SmC^* . In the low-temperature range and on the low-concentration side of the subphase, the characteristic temperature variation of the Bragg reflection peak wavelength could not be well reproduced, as LRILs also play an important role in addition to the thermal fluctuations. In any case, q_T changes continuously with temperature as given by Eqs. (1) and (2). In contrast, q_T must be fixed in the apparently single subphase in the narrow concentration range, although thermal fluctuations also play an important role as it is placed between the states with q_T that changes continuously with temperature. As Sandhya *et al.* [29] suggested, the subphase must be either $q_T = 1/3$ or $1/2$ that is stabilized in an exceptionally wide temperature range. Quite recently, Feng *et al.* [32] studied its dielectric properties in detail and concluded that the subphase is surely the antiferroelectric $q_T = 1/2$ subphase with the four-layer unit cell emerging over a wide temperature range from ~ 80 down to -30°C or lower.

In the following, we have studied the response to an applied electric field in this peculiar $q_T = 1/2$ subphase by two methods and tried to understand the role played by thermal fluctuations; one is the observation of optical rotatory power (ORP) and field-induced birefringence (EFIB) with a setup based on a photoelastic modulator (PEM), and the other is the detection of field-induced ferroelectric polarization with a second-harmonic-generation (SHG) microscope. It was anticipated that the regular (FAFA) unit cell structure in the subphase might be disturbed to some extent by thermal fluctuations so that the electric-field-induced switching was expected to occur layer by layer but not cooperatively and might show a TLAF property even in the bulk [34]. Actually, however, the thermal fluctuations play an important role in promoting the director flip-flopping in a single layer under the applied field and bring about additional induced polarization, which counteracts the ordinary induced polarization and prevents the helix from unwinding; hence, any TLAF property has not been observed in the bulk. At the same time, the director flip-flopping suggests that the Langevin-like director reorientation is the mechanism of the V-shaped switching in thin films as detailed in the following [11,12].

II. EXPERIMENTS

Experimental details of measuring EFIB and ORP by using a photoelastic modulator (PEM-90, Hinds Instruments) were given in previous papers [35–38]. The light source used for EFIB and ORP measurements was a He-Ne laser (633 nm). We followed the conventions that an electric field was applied along the \hat{y} axis and the EFIB was defined as $\Delta n = n_x - n_y$ as in the previous papers [27,36–38]. During our efforts to observe EFIB precisely, we noticed that it is important to monitor the selective reflection (SR) simultaneously and to control carefully the sample thermal and electrical history by observ-

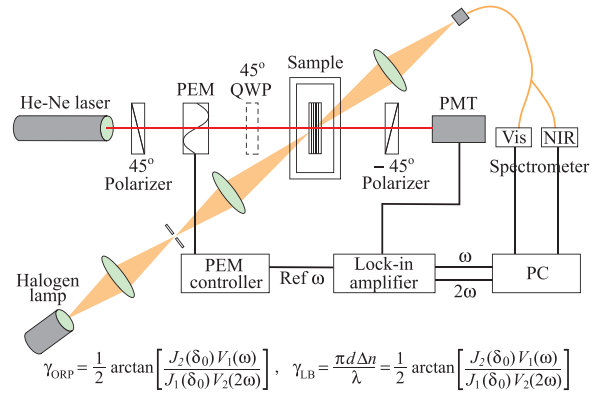


FIG. 3. Optical setup used for measuring EFIB, ORP, and SR. The dashed square stands for a quarter-wave plate (QWP) removed during EFIB (LB) measurement.

ing optical rotatory power (ORP). In the SR measurement, the incident light irradiates the sample at an oblique angle of 20° to observe both the half- and full-pitch Bragg reflection bands. Two spectrometers with 400–1050 and 1000–2400 nm detection ranges are connected by a fiber optic splitter to achieve a wide detection range from visible to near-infrared; an aperture is inserted between the inlet of the fiber and the spectrometer to control the light intensity. These optical properties were studied mainly with a setup developed by Feng and Ishikawa [38] and illustrated in Fig. 3.

In addition to the above conventional methods of studying EFIB, ORP, and SR, we also tried to directly observe field-induced ferroelectric polarization by using second harmonic generation (SHG) so that we might check how uniformly or nonuniformly the polarization is generated in a cell. Figure 4 illustrates a used transmission SH imaging system based on an inverted microscope (Eclipse Ti, Nikon). The fundamental light was a pulsed light of 800 nm wavelength from a fs-Ti:sapphire laser (Vitesse, Coherent) with a repetition

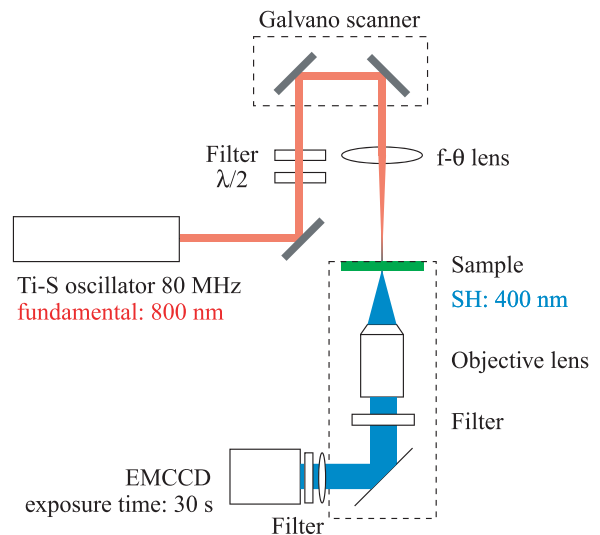


FIG. 4. Schematic illustration of the SHG microscope used. See text for details.

rate of 80 MHz. The fundamental light was incident on the sample placed on a stage via a scanning optical system with a two-axis galvano scanner (6220H, Cambridge Technology) and an f-theta lens (S4LFT0089, Sill Optics). The scanning area is about $0.4 \text{ mm} \times 0.4 \text{ mm}$, and the horizontal and vertical scanning frequencies are 200 and 4 Hz, respectively. The SH light signal generated from the sample was observed by an objective lens (LPlan EPI 50 \times CR, NA = 0.70, Nikon), filtered to remove the fundamental light, and imaged with an Electron Multiplying-CCD (EMCCD) (iXon3, Andor Technology) thermoelectrically cooled down to -65°C and attached to the inverted microscope. The spatial resolution of our SHG microscope is approximately $0.5 \mu\text{m}$. The cell was placed in a homemade hot stage and the temperature was controlled by a temperature controller (HA900, RKC Instrument Inc.).

Materials used were binary mixtures of antiferroelectric MC881(3) containing 54.98, 55.25 and 55.70 wt.% ferroelectric MC452(5). For studying applied electric field effects in the antiferroelectric $q_T = 1/2$ subphase, homeotropically aligned liquid-crystalline cells were constructed so that smectic layers are parallel to the cell surfaces; the homeotropic alignment was achieved by spin-coating JALS204 (JSR Corp.) on the substrates. Copper films of $30 \mu\text{m}$ thickness cut by a sharp knife were used as electrodes and spacers, unless otherwise stated; the electrode separation was adjusted to be around $100 \mu\text{m}$. The material was injected into the cell in the isotropic phase by the capillary effect and slowly cooled down to the $q_T = 1/2$ subphase at room temperature with a temperature-changing rate of $5^\circ\text{C}/\text{h}$ or less. To confirm the stable existence of the $q_T = 1/2$ subphase, we first checked the ORP as a function of temperature as shown in Fig. 5. Two heating and cooling results consecutively measured almost coincide with one another, although clear thermal hysteresis is observed and ORP itself appears to fluctuate intrinsically. The transition temperature between the $q_T = 1/2$ subphase and the SmC^* -like state with continuous q_T is higher in the heating measurements than in the cooling ones [32]. It should be noted that the almost constant ORP observed from RT up to about 80°C indicates the stable existence of the $q_T = 1/2$ subphase. The reason why a sharp ORP increase observed in Fig. 5(a) almost disappears in Fig. 5(b) will be explained in Sec. IV A.

III. RESULTS

A. Transition from $1/2$ to unwound SmC^* and its reverse process as observed by EFIB and ORP

As explained in Sec. I, thermal fluctuations play an important role in the $q_T = 1/2$ subphase under consideration. Since the regular (FAFA) unit cell structure in the subphase might be disturbed to some extent by thermal fluctuations so that a TLAF property was expected to occur at high temperatures even in the bulk, we studied the response to a field at 75°C , i.e., about 5°C below the transition temperature to the SmC^* -like state with continuous q_T . The result is shown in Fig. 6(a). The sample was carefully prepared as specified in Sec. II. An electric field E was applied stepwise with a $10 \text{ mV}/\mu\text{m}$ increment and a 20 s holding time per step; this

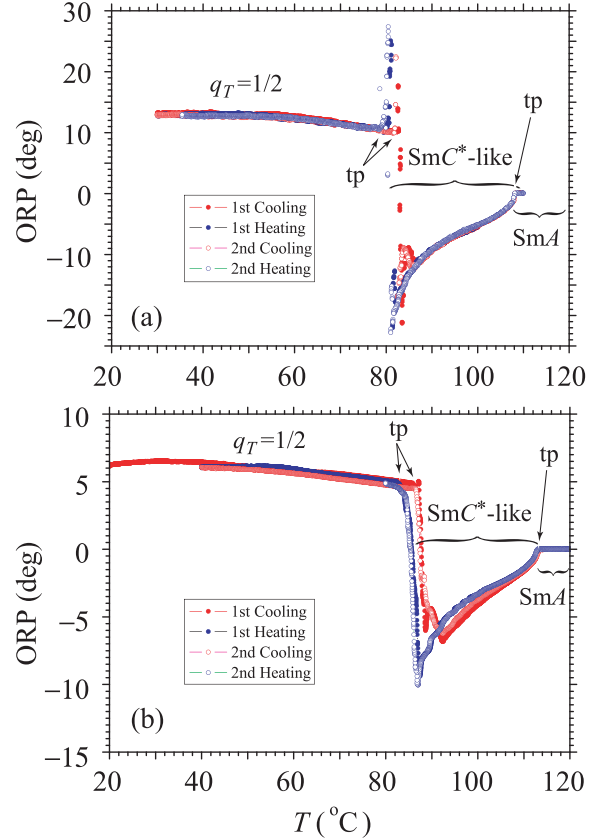


FIG. 5. ORP vs temperature T in MC881 mixtures containing MC452; the concentrations, heating and cooling rates, and sample thicknesses were: (a) 55.25 wt.%, $1^\circ\text{C}/\text{h}$, and $30 \mu\text{m}$; and (b) 55.70 wt.%, $3^\circ\text{C}/\text{h}$, and $14.5 \mu\text{m}$, respectively. We can see $q_T = 1/2$, SmC^* -like state with continuous q_T , and SmA ; tp indicates the transition point between them. See text for details.

way of applying E appeared to be gentle enough. The EFIB stays at $\Delta n \lesssim 2 \times 10^{-3}$ for $E \lesssim 0.15 \text{ V}/\mu\text{m}$, then increases sharply, and attains the saturated value in the ferroelectric unwound SmC^* phase. Likewise, the Bragg reflection intensity stays almost constant for the small Δn range, decreases during the steep Δn increase, and then becomes zero in unwound SmC^* as illustrated in Fig. 6(b). The peak wavelength scarcely changes during these processes. Even when the overall change appears to be continuous as in Fig. 6, the texture observation in unwound SmC^* revealed orientational disorders, which indicates that the field induced transition from $1/2$ to unwound SmC^* did not ideally occur layer by layer as will be discussed in detail in Sec. IV B.

In fact, the Δn - E behavior during its sharp increase is quite unstable. When the holding time in Fig. 6(a) was reduced from 20 s, we obtained Fig. 7(a) where the measurement was first made at a holding time of 20 s, then 5 s, and finally 10 s; after each measurement we observed the sample with an optical microscope and noticed that the orientational disorders became worse through repeated measurements. Figure 7(b) illustrates Δn - E at 30 and 50°C with a $25 \text{ mV}/\mu\text{m}$ increment and a 20 s holding time per step. The range of small Δn becomes narrower with rising temperature. Two consecutive measurements were made at each temperature; the time lag between

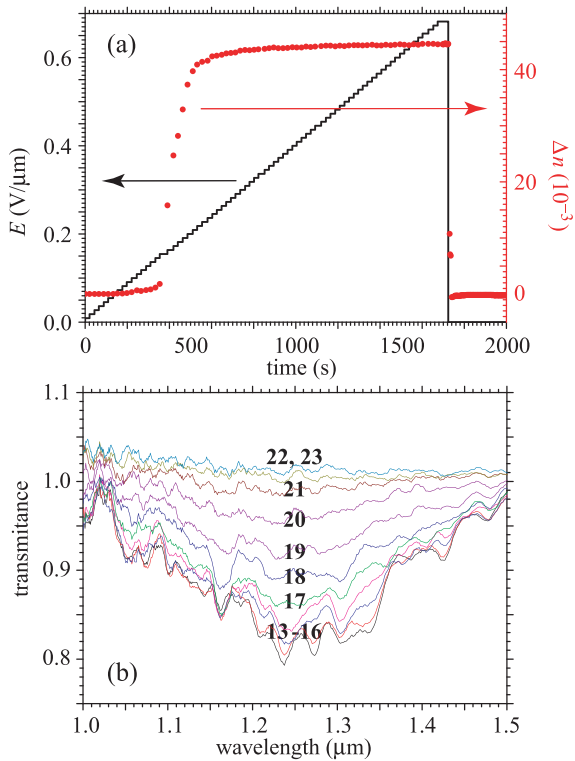


FIG. 6. (a) EFIB Δn and (b) Bragg reflection (Transmittance I_{BR}) spectra of the 55.70 wt.% MC452 mixture at 75°C. An electric field E was applied stepwise with a 10 mV/ μm increment and a 20 s holding time per step. In the Bragg reflection spectra, Nos. 13–16 were for $\Delta n \approx 0$, Nos. 17–21 through the sharp increase range, and Nos. 22 and 23 at almost saturated Δn for unwound SmC*^{*}; the 13th and 23rd steps are 0.12 and 0.21 V/ μm , respectively, as seen in panel (a).

the first and second runs was more than half a day. Once the higher field is applied over the unstable behavior and unwound SmC*^{*} is realized, optical microscope observation clarifies that some alignment defects are produced in the sample cell and these do not disappear even after half a day has passed with the field turned off. When the applied field is lower and does not cause any unstable behavior, the sample simply returns to its original state at $E = 0$ V/ μm almost immediately and no orientational disorder is introduced. It should be noted that the Δn - E curve in the low field region shows a small increase which becomes larger with rising temperature as shown in Fig. 8; the field E was applied stepwise with a 7 mV/ μm increment and a 15 s holding time per step.

Figure 9 shows the field dependence of ORP and its relaxation after switching off the field E studied at 30°C. The setup with the quarter-wave plate illustrated in Fig. 3 is sensitive not only to the optical rotatory power due to the circular birefringence, γ_{ORP} , but also to the retardation due to the linear birefringence, γ_{LB} ; when we use the lock-in amplifier output voltages $V_1(\omega)$ and $V_2(2\omega)$, however, γ_{LB} becomes zero as $V_1(\omega) \equiv 0$ for linear birefringence. In fact, as seen in Fig. 9(a), the $q_T = 1/2$ subphase stably exists with an appropriate pitch. With an increase in the field, the helical pitch becomes longer and hence the ORP increases. As the field is increased further, the helix unwinds itself in a rather complicated way and the

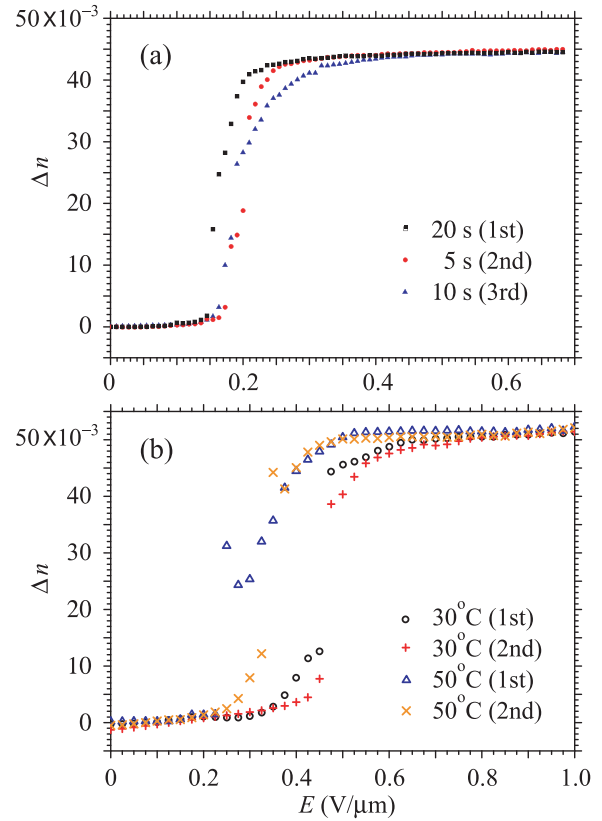


FIG. 7. Unstable behavior of EFIB in its sharp increase region: (a) Δn - E for 5 and 10 s holding times of the 55.70 wt.% MC452 mixture at 75°C, and (b) Δn - E at 30 and 50°C of the 55.25 wt.% MC452 mixture; two consecutive measurements were made at each temperature.

ORP goes to zero. In this way, we demonstrate how the ORP becomes zero as the helix is completely unwound by the field E . When we turn off E with confirming ORP = 0, the ORP suddenly becomes negative and then jumps from negative to positive. The temporal change during $t \lesssim 20$ s is rather fast; after switching off the field, the first and second points are

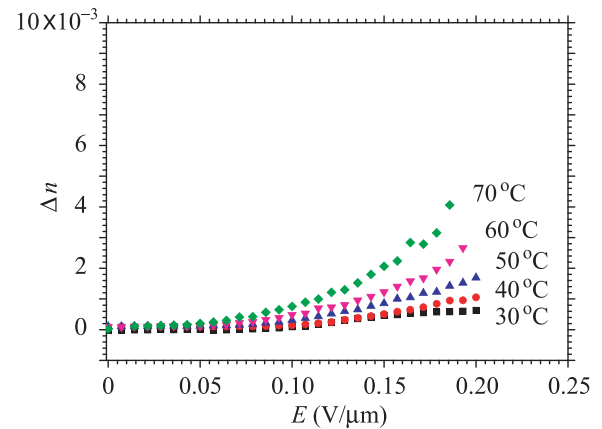


FIG. 8. A small increase of Δn with E in the low field region which becomes larger with rising temperature. The sample used is the 55.70 wt.% MC452 mixture.

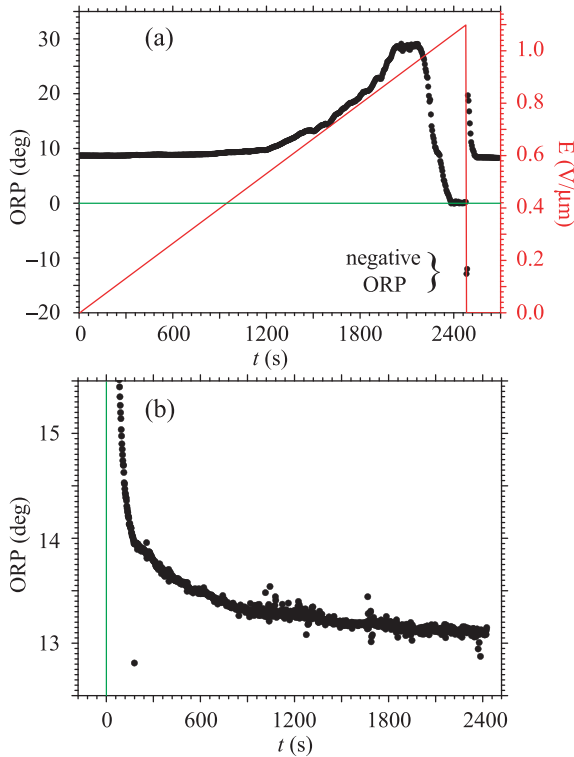


FIG. 9. ORP vs applied field E and its relaxation after turning off E observed at 30°C ; the MC452 concentrations and sample thicknesses were: (a) 54.98 wt.% and about $20\ \mu\text{m}$, and (b) 55.25 wt.% and about $30\ \mu\text{m}$, respectively. See text for further details.

negative, the 3rd point jumps up to a large positive value, and the ORP starts to return to its original $q_T = 1/2$ value. The jumping of observed points infer the characteristic relaxation process from ferroelectric unwound SmC^* with $q_T = 1$ to the antiferroelectric $q_T = 1/2$ subphase as will be detailed in Sec. IV A. In short, the negative ORP shows that the helical structure of almost SmC^* with $q_T \approx 1$ is formed rather quickly within a few seconds, and the extremely scattered data points suggest that q_T passes through the anomalous dispersion area in Fig. 5(a), fluctuating violently in the early stage of relaxation process. After attaining its largest value, the ORP starts to return to its original $q_T = 1/2$ value. In the ORP scale of Fig. 9(a), the relaxation process appears to be completed after a few minutes. When the scale is expanded as in Fig. 9(b), evidently, the ORP does not return to its original virgin value even after 1 h and the thermal fluctuation is much larger than the equilibrium value.

B. Direct observation of field-induced ferroelectric polarization by using an SHG microscope

We now try to directly observe ferroelectric polarization induced by an applied electric field at 50°C . Figure 10 shows images under several fields at a step of 0.05, 0.1, or 0.2 $\text{V}/\mu\text{m}$ from 0 to 1.2 $\text{V}/\mu\text{m}$. Double-headed arrows at the top indicate the polarization direction of the incident light; the field was applied vertically in the figure and its increasing rate was about the same as used in obtaining Fig. 6. It stayed at a particular field for 120 s to take two images for the parallel and

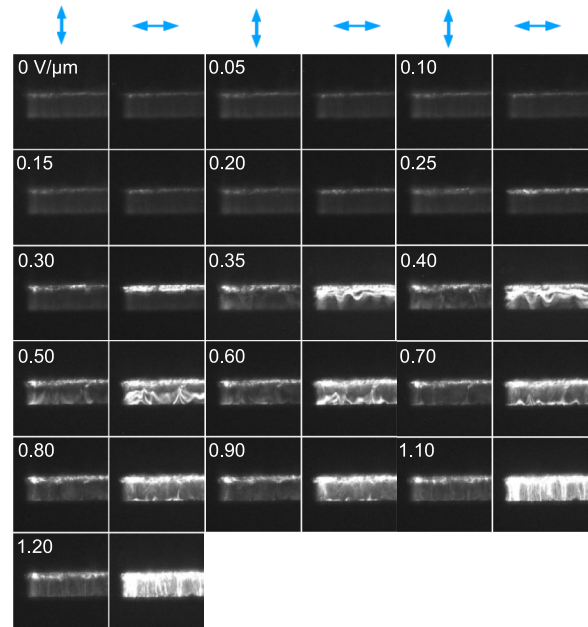


FIG. 10. SHG microscope images for various applied fields observed at 50°C in the 55.25 wt.% MC452 mixture. The exposure time of each image was 60 s and the polarization direction of the fundamental light was specified by double-headed arrows at the top; the field was applied vertically in the figure.

perpendicularly polarized incident lights, as the exposure time of the EMCCD was 60 s. When the field is less than 0.2 $\text{V}/\mu\text{m}$, the electrode edges of the cell are only slightly bright for both incident polarizations. As the field becomes stronger, images become brighter at 0.25~0.3 $\text{V}/\mu\text{m}$, the brightness grows sharply and then appears saturated with further increasing the field; the large fluctuations in saturated values may result from some alignment defects produced in unwound SmC^* as will be discussed in Sec. IV B. The incident light polarized perpendicularly always generates a stronger SH signal than that polarized parallel to the applied field. The plot of SH intensity versus applied field, $I_{\text{SH}}-E$, is shown in Fig. 11. Here the SH

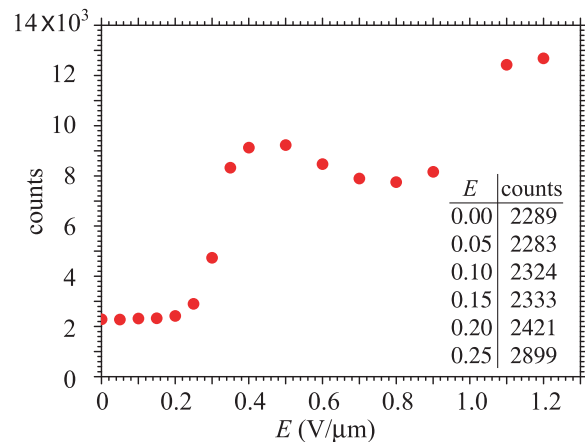


FIG. 11. SH intensity (averaged pixel counts) vs applied field, $I_{\text{SH}}-E$, obtained from the images for the fundamental light polarized perpendicularly to the field in Fig. 10. See text for further details.

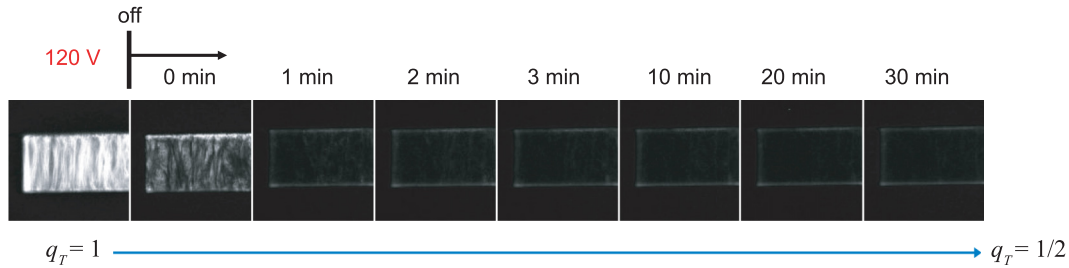


FIG. 12. Temporal change of SHG microscope images after switching off the applied field of $1.50 \text{ V}/\mu\text{m}$ observed at 50°C in the 55.25 wt.% MC452 mixture. The left image was first taken by applying the field, and then a series of images were obtained after switching off the field; the exposure time was 30 s and the polarization direction of the fundamental light was perpendicular to the field.

intensity is the mean gray level in the liquid-crystal portion of each image, which was obtained by using ImageJ [39] to average the pixel counts of each image stored in the EMCCD. Notice that I_{SH} increases slightly even in the low field of $E \leq 0.25 \text{ V}/\mu\text{m}$ as listed on the right side of Fig. 11; the dynamic range of the EMCCD used is 16 bits.

Figure 12 shows the SH image relaxation after the applied field is turned off. It was observed with a different cell from the one used in taking images of Fig. 10, which has a slightly narrow electrode gap of about $80 \mu\text{m}$. At first, 120 V , i.e., $1.50 \text{ V}/\mu\text{m}$, was applied and the SH image was obtained with the SHG microscope. Then a series of images were taken at an elapse of $t = 0, 1, 2, \dots$ min after switching off the field. The polarization direction of the fundamental light was perpendicular to the field, the exposure time 30 s, and the measured temperature 50°C ; the field was applied vertically in the figure. Figure 13 is the corresponding temporal variation of SH intensity; the mean gray level of each image in Fig. 12 was similarly obtained as explained above in connection with Figs. 10 and 11.

We pointed out in Sec. III A that some alignment defects are produced in the sample cell and do not disappear for a long time after switching off the field, but did not show any micrographs. Here we show two pairs of bright-field images of the cells taken by the EMCCD of the SHG microscope using LED lighting with a 0.1 s exposure time. The first pair were taken

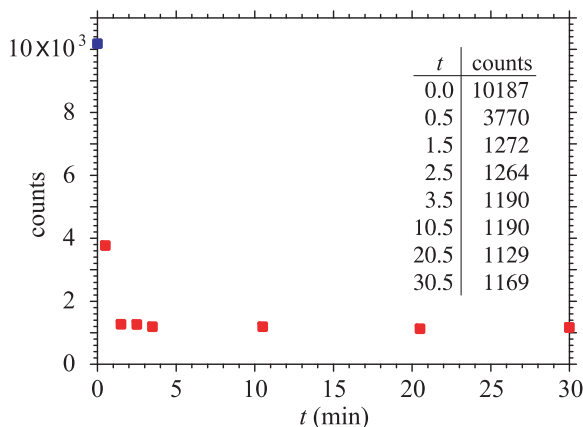


FIG. 13. SH intensity vs time (min), $I_{\text{SH}}-t$, obtained from Fig. 12. Here, the SH intensity is the mean gray level obtained from the images of Fig. 12. See text for further details.

before obtaining images in Fig. 10. The sample was carefully prepared as explained in detail in Sec. II, stored at RT (27°C), and its micrograph was taken as shown in Fig. 14(a). To take SH images in Fig. 10, the sample temperature was carefully raised from RT to 50°C , and its micrograph was obtained as shown in Fig. 14(b). No significant defects are seen in both bright-field images; this means that the cell quality is assured so long as its temperature changes slowly enough. The second pair were taken before and after obtaining images in Fig. 12. Likewise in Figs. 14(a) and 14(b), no significant defects are seen before the measurements as shown in Fig. 14(c) which was obtained without applying the field of $1.50 \text{ V}/\mu\text{m}$. So long as looking at the temporal change of SH images in Fig. 12, the induced polarization almost disappears at 30 min and apparently the cell looks quite uniform. When we obtain the bright-field image of the cell, however, we noticed that alignment defects are actually produced in the sample cell as illustrated in Fig. 14(d). These defects do not disappear for a long time after switching off the field; to remove these defects, we need to repeat the sample preparation process: it is heated up to the isotropic phase and cooled down to RT slowly enough.

IV. DISCUSSIONS

A. ORP and relaxation from ferroelectric unwound SmC^* to antiferroelectric $1/2$

As shown in Fig. 5, the mixtures used have the $q_T = 1/2$ subphase and the SmC^* -like state with continuous q_T ; $q_T > 1/2$ monotonically increases up to 1 with rising temperature and the helical pitch varies with q_T as illustrated in Fig. 13 of

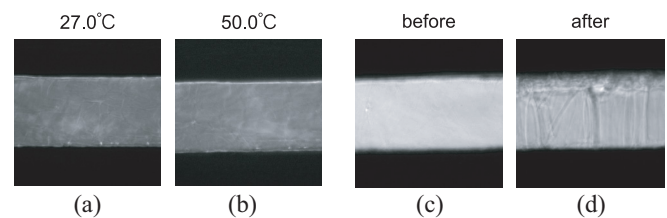


FIG. 14. Bright-field images of the cells taken by the EMCCD of the SHG microscope using LED lighting: panels (a) and (b) were the cell micrographs before obtaining images in Fig. 10, and panels (c) and (d) were taken without applying the field of $1.50 \text{ V}/\mu\text{m}$ and after observing the relaxation process in Fig. 12, respectively. See text for details.

Ref. [29]. The $1/2$ subphase is right handed, whereas wound SmC^* is left handed, in their stable (thermal equilibrium) helical structures, as both MC881 and MC452 used are the (R) moieties [29]; hence their ORPs are positive and negative, respectively, since both characteristic reflection bands appear at wavelength longer than the He-Ne laser (633 nm). The ORP may show the typical anomalous dispersion as illustrated in Fig. 5(a), where it is positively very large and then becomes negative with rising temperature. The positive large ORP part may disappear as in Fig. 5(b), since the minimum q_T value in the SmC^* -like state with continuous q_T critically depends on the MC452 concentration. It is an interesting future problem to clarify the details of the transition behavior between the $q_T = 1/2$ subphase and the SmC^* -like state with continuous q_T ; the intriguing mesoscopic phenomena we are studying result from the degeneracy lifting caused by LRILs with thermal fluctuations playing an important role.

Now we contemplate the relaxation process after switching off the applied field as given in Fig. 9. The observation of large negative ORP during $t \lesssim 10$ s suggests that unwound SmC^* with $q_T = 1$ rather quickly relaxes to a helical SmC^* -like state with reasonably large variable q_T ; notice that wound SmC^* with $q_T = 1$ shows negative ORP as pointed out above. This is consistent with the fact that about 40% ferroelectric spontaneous polarization still remains in the first 30 s as seen in Fig. 13, and hence q_T must be reasonably larger than $1/2$ [32]. Since the state is far separated from the equilibrium just after the electric field was turned off, q_T changes rapidly in the first 30 s or so; even in such situations, the helical pitch and hence ORP must primarily be determined by q_T . In fact, the subsequent ORP steep increase to a large positive value, i.e., the extremely scattered data points suggest that q_T itself also rapidly decreases after field switching off and passes through the anomalous dispersion area in Fig. 5(a), fluctuating violently in the early stage of relaxation process; the helical pitch and hence ORP sensitively depends on q_T near the anomalous dispersion area, where the helical pitch diverges and its handedness changes [29,38]. As q_T approaches $1/2$, its rate of change slows down, and the helical pitch, i.e., ORP, does not change much. Since LRILs are not strong enough, it takes rather long time to almost realize the original virgin ORP value in the $q_T = 1/2$ subphase with the (AFAF) unit cell structure; even in the thermal equilibrium, moreover, ORP is fluctuating intrinsically [29,32].

B. Transition from antiferroelectric $1/2$ to ferroelectric unwound SmC^* and flip-flopping from L to R

Now we move on to the transition from the antiferroelectric $1/2$ subphase to ferroelectric unwound SmC^* induced by an applied field. Contrary to anticipation in a previous paper [34], the response in the bulk illustrated in Figs. 6–8 is quite different from the V-shaped switching which was actually observed in the thin films of Mitsui mixture [11,12] and must have been used in prototyped TLAFLCDs [15–20]. In fact, the helical structure of $1/2$ resists being deformed to keep $\Delta n \approx 0$ when the applied field is low, and then the thresholdlike steep increase of Δn occurs in the transition from $1/2$ to unwound SmC^* . At the same time, this behavior is quite different from that of the ordinary antiferroelectric

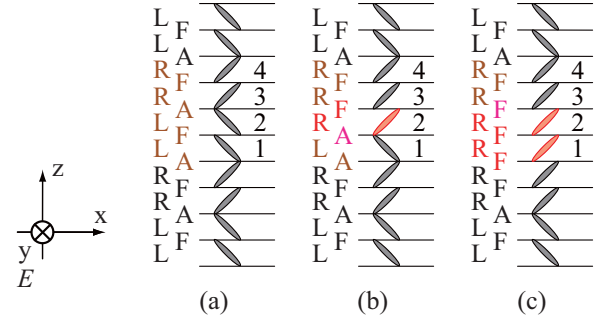


FIG. 15. In the case of (a) the antiferroelectric $q_T = 1/2$ subphase with the four-layer (FAFA) unit cell, (b) additional induced polarization can be produced without changing $q_T = 1/2$ by flop-flipping L in layer 2 to R ; (c) when the flip-flopping occurs in layers 1 and 2, q_T may increase from $1/2$ toward 1. The field is applied in the positive \hat{y} direction and the material has positive polarization. See text for further details.

SmC_A^* and $1/2$ (sub)phases; usually the helical structure starts to unwind from the beginning, and the averaged tilt plane direction tends to be parallel to the applied field so that $\Delta n = n_x - n_y$ becomes negative. It is well established that some nonplanar asymmetric distortion in the antiferroelectric unit cell structure produces induced polarization in the applied field direction, which is observed as the pretransitional effect in the unwound antiferroelectric phase [9,10,40–44].

Why does the antiferroelectric $q_T = 1/2$ subphase in the MC881-MC452 mixtures under consideration behave so characteristically that $\Delta n \approx 0$ when the applied field is low? We should remind us, once again, that the subphase is stabilized by LRILs with thermal fluctuations playing an important role. In the case of the antiferroelectric $q_T = 1/2$ subphase with the four-layer (FAFA) unit cell, thermal fluctuations can produce additional induced polarization without changing $q_T = 1/2$ as illustrated in Fig. 15(b). Since the applied field selectively determines the director tilting sense, we should use

$$q_E = |[R] - [L]| / ([R] + [L]) \quad (3)$$

instead of q_T in Eq. (1). Here $[R]$ and $[L]$ refer to the numbers of smectic layers with directors tilted to the right and to the left, respectively, in the unit cell [44]; to treat helical (sub)phases, the definition is expanded so that R or L produces polarization which has a component parallel or antiparallel to the applied field. An important role played by the flip-flopping between L and R is described by a ratio of electric aligning energy, $p_{\text{eff}} E \cos \phi$, to thermal agitating energy, $k_B T_{\text{eff}}$,

$$p_{\text{eff}} E \cos \phi / (k_B T_{\text{eff}}), \quad (4)$$

where ϕ is the azimuthal angle and $\phi = 0$ corresponds to the \hat{x} axis [11]. Since the change illustrated in Fig. 15(b) makes the ferroelectric (RRRL) unit cell from the antiferroelectric (RRLL) one with maintaining $q_T = 1/2$, thermal fluctuations promote flip-flopping from L to R under the applied low field and may bring about additional induced polarization, which tends to make the averaged tilt plane direction perpendicular to the applied field, compensates for the aforementioned ordinary induced one, and prevent the helical structure starting to unwind from the beginning. In fact, $I_{\text{SH}}-E$ in Fig. 11 indicates

that the field-induced polarization increases with E even in the low field region and the corresponding small increase of Δn with E in Fig. 8 which becomes larger with rising temperature suggests the importance of flip-flopping from L to R due to thermal fluctuations. The helical pitch is mainly determined by $q_T = 1/2$ and hence may not change much as actually observed in Fig. 6(b).

As the applied field becomes higher and the number of additional favorable R increases, the flip-flopping may occur in the same unit cell as illustrated in Fig. 15(c). In other words, the applied field makes the F -ordering more stable than the A -ordering and the ratio $[A]/[F]$ given by the Boltzmann distribution in Eq. (2) diminishes from 1 by changing the $[A]$ ordering to the $[F]$ ordering, so that q_T may increase from $1/2$ toward 1 [29]. The change may occur in a nonuniform defect-assisted way through solitary waves moving around dynamically as the system is thermally fluctuating [33,45,46]; it facilitates the field-induced transition to unwound SmC^* so that Δn increases steeply and the Bragg reflection intensity diminishes as shown in Fig. 6. When unwound SmC^* is almost realized, some 2π walls may disturb Δn in attaining the real saturation as actually observed in Fig. 7 [47,48]. Basically, these solitary waves and 2π walls are closely related with defects or imperfect boundaries and may easily be trapped there, and cause orientational disorders after performing experiments as shown in Fig. 14. Therefore, if we could make a cell that satisfies the perfect condition of no imperfections, then we may observe more uniform SH images than those given in Fig. 10.

The SHG microscope system in Fig. 4 is so sensitive that it can detect polarization induced by an applied field without changing $q_T = 1/2$ as illustrated in Fig. 15(b). The motive for this study comes from a previous report that the system is useful to detect the flexoelectric polarization produced in nematic liquid crystals [49]. No SHG is observed in a uniformly aligned nematic cell because of the $D_{\infty h}$ symmetry; when an applied field deforms it locally and produces flexoelectric polarizations, a weak SH light can visualize them. On the contrary, ferroelectric liquid crystals (FLCs) with the C_2 symmetry have spontaneous polarization and are subject to SHG. It has been shown that the SHG light intensity has a correlation with the spontaneous polarization [50]; the contribution from the spontaneous polarization along the C_2 axis is dominant and hence the incident light polarized parallel to the applied field may give the strongest SHG. Actually, however, angle phase matching occurs only for the incident light polarized perpendicularly to the applied field [51] and the stronger SHG is observed for the incident light polarized perpendicularly as indicated in Fig. 10. It should be noted that AFLC has a noncentrosymmetric structure of D_2 symmetry and is SHG active [52]. Although no detailed study has been made so far, the antiferroelectric $q_T = 1/2$ subphase under consideration gives a very weak SH light, which might contribute some small background at $E = 0 \text{ V}/\mu\text{m}$ in Fig. 11.

C. Conclusions and future plans

In spite of the anticipation that the very characteristic $q_T = 1/2$ subphase under consideration might exhibit TLAf property in the bulk, its helical structure resists being deformed

by an applied electric field and any TLAf properties are not observed; at the same time, however, the thermal fluctuations play an important role in promoting flip-flopping between L and R orderings of a single layer under the applied field. In a homogeneously aligned (smectic layers \perp substrate plates) thin cell the interfaces may destroy the helix and realize the uniformly aligned $q_T = 1/2$ subphase with the four-layer $RRLL$ (FAFA) unit cell as illustrated in Fig. 15(a). Since it has the distortion angle δ [23,53,54] and the directors are not really parallel to the substrate plates, the sum of bulk and surface energies may prefer the much simpler two-layer RL (FA) unit cell of SmC_A^* . Moreover, the thermally promoted flip-flopping between L and R may help the change from the four-layer unit cell structure to the two-layer one and produce some randomization in the $q_E = 0$ uniformly aligned structure.

A crucial but still unclear aspect is the detailed mechanism by which substrate interfaces induce an ordered or disordered state different from that in the bulk and responsible for the emergence of TLAf in homogeneously aligned thin cells. In any case, the distribution of local in-plane directors must be at least approximately given by

$$f(\phi) = \frac{1}{2\sqrt{2\pi}\sigma} \left\{ \exp\left(-\frac{\phi^2}{2\sigma^2}\right) + \exp\left(-\frac{(\phi - \pi)^2}{2\sigma^2}\right) \right\}. \quad (5)$$

Here σ is the standard deviation and $\phi = 0$ corresponds to the \hat{x} axis in Fig. 15. The flip-flopping between L and R plays an important role, the Langevin-like director reorientation may be caused by an applied field, and the V-shaped switching is expected to appear as a TLAf property [11,12], which was actually confirmed in thin cells of Mitsui mixture by Raman scattering and must have been used in prototyped TLAf-LCDs [15–20]. Unfortunately, the bulk properties of the Mitsui mixture have not been studied in as much detail as those of the MC881-MC452 mixtures. In thin cells, however, the situation is just opposite; any detailed systematic investigations have not been performed yet in the MC881-MC452 mixtures, although Song *et al.* [55], without knowing the existence of the antiferroelectric $q_T = 1/2$ subphase, reported the TLAf-like response in a $2\text{-}\mu\text{m}$ thick cell of the MC881 mixture containing 55 wt.% MC452 by observing apparent polarization as a function of applied field. We would like to directly observe in thin cells the subphase structure by resonant x-ray scattering, the field-induced ferroelectric polarization with the SHG microscope, and the relaxation frequency of the flip-flopping between L and R by photon correlation spectroscopy in the near future [56].

ACKNOWLEDGMENTS

MGC is acknowledged for the gift of precious liquid-crystal compounds, MC881 and MC452. The authors thank Zhengyu Feng, a former graduate student at Tokyo Tech, for his help during the experiments at the early stage of this study. We also thank to Fumito Araoka at RIKEN for providing the experimental setup for SH imaging and for helpful discussions. Part of this work was supported by JSPS KAKENHI Grant No. JP19K05247. N.Y. thanks the Irish

Research Council for the award of PDF GOIPD/2021/858. V.P.P. thanks the NRF, Korea for funding of the Creative Challenge project (Grant No. NRF-2021R1I1A1A01061278).

J.K.V. thanks the Science Foundation Ireland Proposal (ID No. 21/US/3788) for part funding of the work in Dublin.

- [1] A. Fukuda, Pretransitional effect in AF-F switching: To suppress it or to enhance it, that is the question about AFLCDs, in *Proceedings of the Fifteenth International Display Research Conference* (Asia Display '95, Hamamatsu, 1995), p. 61.
- [2] C. Tanaka, T. Fujiyama, T. Maruyama, and S. Nishiyama, Antiferroelectric liquid crystal with a novel hysteresis loop, in *Proceedings of Japanese Liquid Crystal Society Annual Meeting*, Sendai, 1995, p. 250 [in Japanese].
- [3] S. Inui, N. Imura, T. Suzuki, H. Iwase, K. Miyachi, Y. Takanishi, and A. Fukuda, Thresholdless antiferroelectricity in liquid crystals and its application to display, *J. Mater. Chem.* **6**, 671 (1996).
- [4] P. Rudquist, J. P. F. Lagerwall, M. Buivydas, F. Gouda, S. T. Lagerwall, N. A. Clark, J. E. Maclennan, R. Shao, D. A. Coleman, S. Bardon, T. Bellini, D. R. Link, G. Natale, M. A. Glaser, D. M. Walba, M. D. Wand, and X.-H. Chen, The case of thresholdless antiferroelectricity: polarization-stabilized twisted SmC* liquid crystals give V-shaped electro-optic response, *J. Mater. Chem.* **9**, 1257 (1999).
- [5] P. Rudquist, J. P. F. Lagerwall, M. Buivydas, F. Gouda, S. T. Lagerwall, R. F. Shao, D. Coleman, S. Bardon, D. R. Link, T. Bellini, J. E. Maclennan, D. M. Walba, N. A. Clark, and X. H. Chen, Unraveling the mystery of “thresholdless antiferroelectricity”: High contrast analog electro-optics in chiral smectic-liquid crystal, *SID Symposium Digest* **30**, 409 (1999).
- [6] B. Park, S.-S. Seomun, M. Nakata, M. Takahashi, Y. Takanishi, K. Ishikawa, and H. Takezoe, Collective molecular motion during V-shaped switching in a smectic liquid crystal, *Jpn. J. Appl. Phys.* **38**, 1474 (1999).
- [7] B. Park, M. Nakata, S.-S. Seomun, Y. Takanishi, K. Ishikawa, and H. Takezoe, Molecular motion in a smectic liquid crystal showing V-shaped switching as studied by optical second-harmonic generation, *Phys. Rev. E* **59**, R3815(R) (1999).
- [8] S.-S. Seomun, T. Gouda, Y. Takanishi, K. Ishikawa, H. Takezoe, and A. Fukuda, Bulk optical properties in binary mixtures of antiferroelectric liquid-crystal compounds showing V-shaped switching, *Liq. Cryst.* **26**, 151 (1999).
- [9] T. Qian and P. L. Taylor, Field-induced phase transitions in antiferroelectric liquid crystals, *Phys. Rev. E* **60**, 2978 (1999).
- [10] L. A. Parry-Jones and S. J. Elston, Importance of quadrupolar ordering in antiferroelectric liquid-crystal devices, *Appl. Phys. Lett.* **79**, 2097 (2001).
- [11] N. Hayashi, T. Kato, T. Aoki, T. Ando, A. Fukuda, and S.-S. Seomun, Probable Langevin-Like Director Reorientation in an Interface-Induced Disordered SmC*-Like State of Liquid Crystals Characterized by Frustration Between Ferro- and Antiferroelectricity, *Phys. Rev. Lett.* **87**, 015701 (2001).
- [12] N. Hayashi, T. Kato, T. Aoki, T. Ando, A. Fukuda, and S. S. Seomun, Orientational distributions in smectic liquid crystals showing V-shaped switching investigated by polarized Raman scattering, *Phys. Rev. E* **65**, 041714 (2002).
- [13] Y. Yoshioka, M. Johnno, T. Yui, and T. Matsumoto, Liquid crystal composition, European Patent Application EP1039329 (2000).
- [14] T. Matsumoto, Development of the liquid crystal materials showing V-shape switching, in *Program Book of the Eighth International Conference of Ferroelectric Liquid Crystals*, Washington, 2001, I-19.
- [15] T. Saishu, K. Takatoh, R. Iida, H. Nagata, and Y. Mori, Voltage holding properties of thresholdless antiferroelectric liquid crystals driven by active matrix, *SID Symposium Digest* **27**, 703 (1996).
- [16] T. Yoshida, T. Tanaka, J. Ogura, H. Wakai, and H. Aoki, A full-color thresholdless antiferroelectric LCD exhibiting wide viewing angle with fast response time, *SID Symposium Digest* **28**, 841 (1997).
- [17] R. Hasegawa, H. Fujiwara, H. Nagata, T. Saishu, R. Iida, Y. Hara, M. Akiyama, H. Okumura, and K. Takatoh, Novel driving method for thresholdless antiferroelectric liquid crystal display with active matrices, in *Proceedings of International workshop on Active-Matrix Liquid-Crystal Displays*, Tokyo, 1997 (The Japan Society of Applied Physics, Tokyo, 1997), p. 119.
- [18] T. Verhulst, Analytical modelling of active-matrix driving of liquid crystals with spontaneous polarization, *Jpn. J. Appl. Phys.* **36**, 720 (1997).
- [19] M. Lu, K. H. Yang, and J. L. Sanford, V-shaped switching ferroelectric liquid crystal for reflective microdisplay applications, *Ferroelectrics* **246**, 163 (2000).
- [20] L. K. M. Chan, P. Bartelous, P. W. H. Surguy, N. Flannigan, G. Swedenkras, C. Waldelof, M. Rampin, A. Vindigni, I. Underwood, D. G. Vass, M. I. Newsam, J. M. Oton, and X. Quintana, Antiferroelectric microdisplays on silicon, in *Proceedings of the 20th International Display Research Conference*, Palm Beach, 2000 (The Society for Information Display, Campbell, 2000), p. 261.
- [21] MGC considered that these ferroelectric compounds must be ferroelectric because of their characteristic conoscopic behavior. Song *et al.* clearly showed, however, that these are ferroelectric [46].
- [22] A. Fukuda, Y. Takanishi, T. Isozaki, K. Ishikawa, and H. Takezoe, Feature article: Antiferroelectric chiral smectic liquid crystals, *J. Mater. Chem.* **4**, 997 (1994).
- [23] A. V. Emelyanenko and M. A. Osipov, Theoretical model for the discrete flexoelectric effect and a description for the sequence of intermediate smectic phases with increasing periodicity, *Phys. Rev. E* **68**, 051703 (2003).
- [24] P. V. Dolganov and E. I. Kats, Landau theory description of polar smectic structures, *Liquid Crystals Reviews* **1**, 127 (2013).
- [25] C. C. Huang, S. Wang, L. Pan, Z. Q. Liu, B. K. McCoy, Y. Sasaki, K. Ema, P. Barois, and R. Pindak, Liquid crystal mesophases beyond commensurate four periodicity, *Liquid Crystals Reviews* **3**, 58 (2015).
- [26] Z. Feng, A. D. L. Chandani Perera, A. Fukuda, J. K. Vij, K. Ishikawa, A. Iida, and Y. Takanishi, Definite existence of subphases with eight- and ten-layer unit cells as studied by complementary methods, electric-field-induced birefringence and microbeam resonant x-ray scattering, *Phys. Rev. E* **96**, 012701 (2017).

- [27] A. D. L. Chandani Perera, A. Fukuda, J. K. Vij, and Y. Takanishi, Ferrielectric six-layer $q_E = 1/3$ ($q_T = 2/3$) and several electric-field-induced subphases in AS657 studied by complementary methods, electric-field-induced birefringence and microbeam resonant x-ray scattering, *Liq. Cryst.* **44**, 1787 (2017).
- [28] A. Fukuda, J. K. Vij, and Y. Takanishi, Variety of subphase emerging sequences, the frustration of three main interlayer phases, SmC_A^* , SmC^* , and SmA , and the long-range interactions, *Phys. Rev. E* **104**, 014705 (2021).
- [29] K. L. Sandhya, A. D. L. Chandani, A. Fukuda, J. K. Vij, A. V. Emelyanenko, and K. Ishikawa, Degeneracy lifting due to thermal fluctuations around the frustration point between anticlinic antiferroelectric SmC_A^* and synclinic ferroelectric SmC^* , *Phys. Rev. E* **87**, 012502 (2013).
- [30] J. Prost and R. Bruinsma, Fluctuation forces and the devil's staircase of ferro/antiferroelectric smectic C^* 's, *Ferroelectrics* **148**, 25 (1993).
- [31] R. Bruinsma and J. Prost, Fluctuation forces and the devil's staircase of ferroelectric smectic C^* 's, *J. Phys. II France* **4**, 1209 (1994).
- [32] Z. Feng, V. Swaminathan, V. P. Panov, A. Fukuda, K. Ishikawa, and J. K. Vij, Dielectric study of a subphase stabilized in an exceptionally wide temperature range by a delicate balance of interlayer interactions and thermal fluctuations, *Phys. Rev. E* **102**, 012703 (2020).
- [33] J.-K. Song, A. Fukuda, and J. K. Vij, Dynamic Mechanism of the Ferroelectric to Antiferroelectric Phase Transition in Chiral Smectic Liquid Crystals, *Phys. Rev. Lett.* **101**, 097801 (2008).
- [34] A. Fukuda, What are thresholdless antiferroelectric (TLAF) LCS?—disordered SmC^* -like phase with $q_T = 1/2$ in a wide temperature range, *Mol. Cryst. Liq. Cryst.* **610**, 1 (2015).
- [35] M. Škarabot, M. Čepič, B. Zeks, R. Blinc, G. Heppke, A. V. Kityk, and I. Musevic, Birefringence and tilt angle in the antiferroelectric, ferroelectric, and intermediate phases of chiral smectic liquid crystals, *Phys. Rev. E* **58**, 575 (1998).
- [36] N. M. Shtykov, A. D. L. Chandani, A. V. Emelyanenko, A. Fukuda, and J. K. Vij, Two kinds of smectic- C^* subphases in a liquid crystal and their relative stability dependent on the enantiomeric excess as elucidated by electric-field-induced birefringence experiment, *Phys. Rev. E* **71**, 021711 (2005).
- [37] A. D. L. Chandani, N. M. Shtykov, V. P. Panov, A. V. Emelyanenko, A. Fukuda, and J. K. Vij, Discrete flexoelectric polarizations and biaxial subphases with periodicities other than three and four layers in chiral smectic liquid crystals frustrated between ferroelectricity and antiferroelectricity, *Phys. Rev. E* **72**, 041705 (2005).
- [38] Z. Feng and K. Ishikawa, Development of simultaneous measurement system of birefringence, optical rotational power, and transmission spectra for chiral liquid crystal phases, *Jpn. J. Appl. Phys.* **55**, 050301 (2016).
- [39] W. S. Rasband, ImageJ, U.S. National Institute of Health, Bethesda, MD, <https://imagej.nih.gov/ij/>.
- [40] M. Johno, K. Itoh, J. Lee, Y. Ouchi, H. Takezoe, A. Fukuda, and T. Kitazume, Temporal and spatial behavior of the field-induced transition between antiferroelectric and ferroelectric phases, *Jpn. J. Appl. Phys.* **29**, L107 (1990).
- [41] K. Hiraoka, H. Takezoe, and A. Fukuda, Dielectric relaxation modes in the antiferroelectric smectic C_A^* phase, *Ferroelectrics* **147**, 13 (1993).
- [42] L. A. Parry-Jones and S. J. Elston, Field-driven helix unwinding in antiferroelectric liquid crystal cells, *Phys. Rev. E* **63**, 050701(R) (2001).
- [43] J.-K. Song, A. Fukuda, and J. K. Vij, Antiferroelectric dielectric relaxation processes and the interlayer interaction in antiferroelectric liquid crystals, *Appl. Phys. Lett.* **93**, 142903 (2008).
- [44] A. D. L. Chandani, A. Fukuda, J. K. Vij, Y. Takanishi, and A. Iida, Effective long-range interlayer interactions and electric-field-induced subphases in ferrielectric liquid crystals, *Phys. Rev. E* **93**, 042707 (2016).
- [45] J.-F. Li, X.-Y. Wang, E. Kangas, P. L. Taylor, C. Rosenblatt, Y. I. Suzuki, and P. E. Cladis, Reversible propagating fingers in an antiferroelectric liquid crystal, *Phys. Rev. B* **52**, R13075(R) (1995).
- [46] J.-K. Song, A. D. L. Chandani, A. Fukuda, J. K. Vij, I. Kobayashi, and A. V. Emelyanenko, Temperature-induced sign reversal of biaxiality observed by conoscopy in some ferroelectric $Sm-C^*$ liquid crystals, *Phys. Rev. E* **76**, 011709 (2007).
- [47] P. G. de Gennes and J. Prost, *The Physics of Liquid Crystals*, 2nd ed. (Clarendon Press, Oxford, UK, 1993).
- [48] Ph. Martinot-lagarde, Unwinding of the helical texture of smectic C^* liquid crystal, through ferroelectric and dielectric anisotropic coupling with an applied field, *Mol. Cryst. Liq. Cryst.* **66**, 61 (1981).
- [49] K. Shirota, F. Araoka, and Y. Yamagata, Visualization of flexoelectric polarization in liquid crystal cells and its analysis, in *Proceedings of Japanese Liquid Crystal Society Annual Meeting*, Tsukuba, 2019 (The Japanese Liquid Crystal Society, Tokyo, 2019), p. 3C05 [in Japanese].
- [50] A. Taguchi, K. Kajikawa, Y. Ouchi, H. Takezoe, and A. Fukuda, Second harmonic generation in ferroelectric liquid crystals, in *Nonlinear Optics of Organics and Semiconductors*, Springer Proceedings in Physics, edited by T. Kobayashi (Springer-Verlag, Berlin, 1989), Vol. 36, p. 250.
- [51] A. Taguchi, Y. Ouchi, H. Takezoe, and A. Fukuda, Angle phase matching in second harmonic generation from a ferroelectric liquid crystal, *Jpn. J. Appl. Phys.* **28**, L997 (1989).
- [52] T. Fujioka, K. Kajikawa, H. Takezoe, A. Fukuda, T. Kusumoto, and T. Hiyama, Second-harmonic generation in antiferroelectric liquid crystal, *Jpn. J. Appl. Phys.* **32**, 4589 (1993).
- [53] I. Mušević and M. Škarabot, Optical rotation and structure of ferrielectric smectic phases, *Phys. Rev. E* **64**, 051706 (2001).
- [54] M. Čepič and H. F. Gleeson, in *Handbook of Liquid Crystals*, 2nd ed., edited by J. W. Goodby, P. J. Collings, T. Kato, C. Tschierske, H. F. Gleeson, and P. Raynes (Wiley-VCH, Weinheim, 2014), Vol. 4, p. 417.
- [55] J. K. Song, A. Fukuda, and J. K. Vij, Gradual phase transition between the smectic- C^* and smectic- C_A^* phases and the thresholdless antiferroelectricity, *Phys. Rev. E* **78**, 041702 (2008).
- [56] K. Miyachi, M. Kabe, K. Ishikawa, H. Takezoe, and A. Fukuda, Fluctuation in the ferrielectric smectic- C^* phase as observed by laser beam diffraction and photon correlation spectroscopy, *Ferroelectrics* **147**, 147 (1993).